Ablating Ion Velocity Distributions in Short-Pulse-Heated Solids via X-Ray Doppler Shifts

B. F. Kraus, Lan Gao, W. Fox, K. W. Hill, M. Bitter, P. C. Efthimion, A. Moreau, R. Hollinger, Shoujun Wang, Huanyu Song, and J. J. Rocca

Phys. Rev. Lett. **129**, 235001 — Published 2 December 2022

DOI: 10.1103/PhysRevLett.129.235001

Ablating ion velocity distributions in short-pulse-heated solids via x-ray Doppler shifts

B. F. Kraus,[1,2] Lan Gao,[2] W. Fox,[2] K. W. Hill,[2] M. Bitter,[2] P. C. Efthimion,[2]
A. Moreau,[3] R. Hollinger,[3] Shoujun Wang,[3] Huanyu Song,[3] and J. J. Rocca[3,4]

[1]*Department of Astrophysical Sciences, Princeton University, Princeton, New Jersey, USA*
[2]*Princeton Plasma Physics Laboratory, Princeton University, Princeton, New Jersey, USA*
[3]*Electrical and Computer Engineering Department, Colorado State University, Fort Collins, Colorado, USA*
[4]*Physics Department, Colorado State University, Fort Collins, Colorado, USA*

(Dated: November 4, 2022)

Solids ablate under laser irradiation, but experiments have not previously characterized the initiation of this process at ultrarelativistic laser intensities. We present first measurements of bulk ion velocity distributions as ablation begins, captured as a function of depth via Doppler-shifted x-ray line emission from two viewing angles. Bayesian analysis indicates that bulk ions are either nearly stationary or flowing outward at the plasma sound speed. The measurements quantitatively constrain the laser-plasma ablation mechanism, suggesting that a step-like electrostatic potential structure drives solid disassembly.

High-intensity short-pulse lasers produce extreme conditions when focused on solid materials. Not only do the interactions create relativistic electron[1] and ion[2,3] beams, but they also push and heat the bulk solid surface[4] to hot-dense plasma states. Many mechanisms of laser-surface interaction have been studied, including hole boring,[5] laser-driven shock heating,[6] and return-current induction by fast electrons;[7] what is always certain is that the laser ablates the solid, propelling an extended plasma plume outward into vacuum.[8–10] The details of solid material ablation influence all subsequent dynamics, including shock propagation and heat transport through flowing dense plasma, as well as the rate of target disassembly. Despite its ubiquity, how ablation originates at high laser intensities remains an open question. For instance, models of plasma expansion reliably quantify aspects of relativistic ion acceleration,[11,12] but their implications for the electrostatic ablation of surface plasma have not been experimentally validated.

In this Letter, we present the first experimental observations of solid-density plasma flows during the initiation of ablation by an ultrarelativistic laser pulse. Our measurements of Doppler-shifted x-ray lines directly convey the emission-weighted distribution of ion velocities as a function of depth into the solid target. Bayesian analysis indicates that some ions are stationary and others are flowing at the plasma sound speed, with few ions at intermediate velocities. The observed phenomenon is fundamentally distinct from MeV-scale fast ion acceleration, since characteristic velocities are on the order of the bulk plasma thermal velocity; instead, results are consistent with a thin, sheath-like ablation front traveling into the solid that rapidly accelerates the hot dense plasma outward, conflicting with (1) predictions of gradual ablation by most models of plasma expansion[12] and (2) extrapolation to high densities of photon-pressure-driven shocks[6] and hole-boring.[13,14] These measurements are newly possible by coupling high-resolution x-ray crystal spectrometers, which observe line shapes from dense plasmas with unprecedented clarity, to a laser system with ultrahigh contrast that prevents preexpansion and direct laser interaction with observed solid material. Laser targets with thin embedded tracer layers impart spatial resolution to the measurements while limiting the influence of confounding factors such as plasma gradients or radiation transport. The demonstrated technique is new to laboratory high-energy-density physics, here revealing new insights about laser ablation of solids, and could be adapted for general use on other experimental platforms.

Experiments were undertaken at the Advanced Laser for Extreme Photonics (ALEPH),[15] which irradiated foil targets at normal incidence with 8–10 J of wavelength $\lambda = 400$ nm laser light in a pulse of width 45 fs, focused into a near-diffraction-limited spot of ~ 1.5 μm diameter at intensities $> 10^{21}$ W/cm^2. Pulses were frequency-doubled to maximize temporal contrast, limiting prepulse effects (see simulation-based quantification below); high contrast is necessary to prevent direct laser interaction with the tracer layer and maintain solid-density for the duration of the measurement. The laser targeted Al foils (total thickness 20–25 μm) that contained embedded, 125-nm-thick Ti tracer layers, buried a distance z_{Ti} under the laser-facing surface. Though a large fraction[16] of laser energy transfers to relativistic, $\sim$ MeV electrons[17] outside the target at the critical surface, those fast electrons transport energy into the solid, generating return currents[18,19] that heat embedded Ti layers to He-like ionization states and beyond. (Due to finite beam divergence and thick targets, refluxing relativistic electrons are not expected to significantly impact the hot-dense region.[20]) The $n = 2 \rightarrow 1$ transitions in highly charged ions create x-rays energetic enough to escape the solid material; we observe these photons with Bragg-diffracting quartz crystal spectrometers, capable of measurements with high spectral resolution ($E/\Delta E \sim 10^4$).[21] The diagnostic geometry, in-

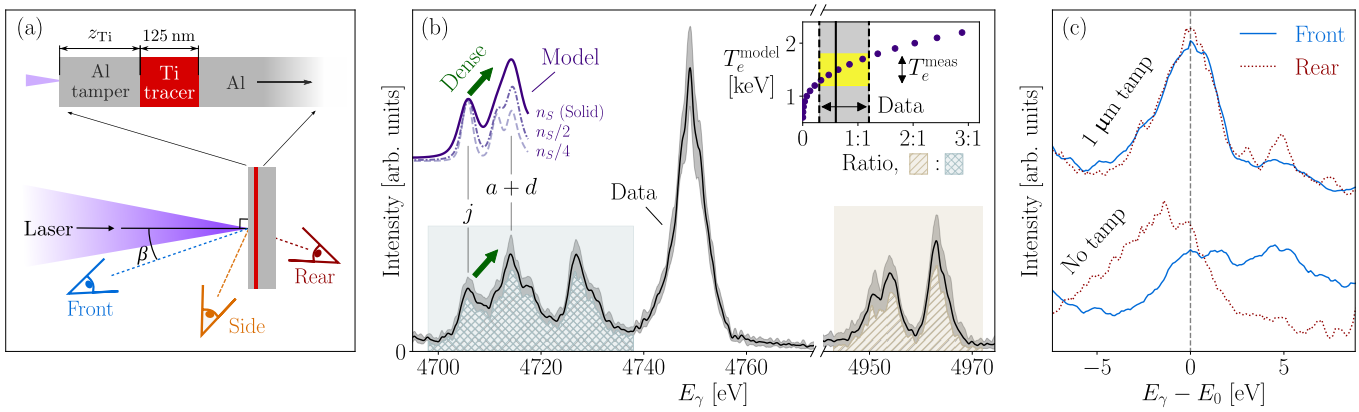

FIG. 1. (a) Cartoon of the experimental setup, including tracer layer targets and three spectrometer views. (b) Front-viewed x-ray spectra versus photon energy E_γ (solid lines/shaded regions are ten-shot means/standard deviations) at $z_{Ti} = 250$ nm with the Ti Heα complex and Lyα resonance lines. Model predictions from the SCRAM code[25] (vertically offset, upper left) show satellite intensity ratios at three labeled densities; similar calculations at different T_e generate the upper right inset, where the shaded band reflects observations. "Ratio" is the line intensity ratio between the hatched regions, notably avoiding opacity effects from the Heα resonance line. (c) IC line shapes, tamped and untamped as labeled, shown from front and rear views.

cluding target and focus location, crystals, and charge coupled device detector, remained fixed in space over repeated laser shots, maintaining the spectrometer dispersion and thus allowing multiple measurements on identical targets to gauge shot-to-shot variation. The stationary setup allows unambiguous comparison of line shifts between targets with different z_{Ti}. Full scans over 0 μm $\leq z_{Ti} \leq$ 1 μm in steps of 125 nm (investigated out of order to prevent systematic errors) were performed from three spectrometer views: $\beta = 22.5°$ ("front"), 67.5°("side"), and 157.5°("rear"), where β is the angle of observation with respect to target normal. Aspects of this experimental setup are summarized in Fig. 1(a).

High-resolution x-ray spectra, as in Fig. 1(b), contain features that change with emitting plasma conditions; here, line intensity ratios imply that observed plasmas are near solid density and hot. These assertions hinge on collisional-radiative atomic kinetic theory,[22] which in specific circumstances predicts proportionality between single plasma parameters and line intensities. For example, when hot Ti plasmas approach solid density ($n_S = 1.2 \times 10^{24}$ e$^-$/cm^3 in He-like Ti), collisions equilibrate Li-like ground states $1s^2 2s$ and $1s^2 2p$, opening new excitation channels for certain $1s2p^2$ states.[23] This effect manifests as relatively intense satellites (a, d)[24] versus others (j), according to the collisional-radiative model SCRAM[25] and indicated in the figure. Measurements *at all observed* z_{Ti} showcase bright, overlapping $a+d$ satellites, intense relative to their low-energy neighbor j; emission-averaged densities are thus $> n_S/2$. (We refrain from specifying best-fit density values due to nonzero Doppler shift contamination and the likelihood of temporal gradients, since the plasma likely begins at solid density before expanding.) In parallel, the ratio of H-like to He-like line emission at near-solid densities is a function almost exclusively of electron temperature T_e. Significant Lyα emission compared to satellites of Heα establishes $T_e \sim 1.5$ keV at $z_{Ti} = 250$ nm, a value which accounts for limited reabsorption (since tracer layers are thin, all lines except the Heα resonance have optical depth $\tau < 1$ according to SCRAM). Relative Lyα intensity gradually decreases with depth but remains significant up to $z_{Ti} \sim 2$ μm. Though calibration of Lyα to Heα intensities relies on theoretical crystal reflectivities,[26,27] line ratios depend so strongly on temperature that a conservative factor-of-two uncertainty in Lyα intensity reduces to ±20% uncertainty in inferred T_e and ±10% uncertainty in the bulk ion sound speed c_s.

Beyond inferences from line ratios, line shapes measured from front and rear views indicate that hot, near-solid-density plasma flows outward, especially near the surface. As shown in Fig. 1(c), line shapes from the He-like Ti intercombination (IC) line are independent of viewing angle when the tracer layer is buried under a thick tamper that restricts plasma expansion. However, these line shapes shift in opposite directions when the tamper layer is removed: front views record line emission at higher energies, and rear views see lower-energy emission. No spectral transition is present at energies just below the IC line,[28] meaning the rear view measurement is inexplicable unless plasma flows away from the spectrometer—away from the laser-facing surface. In fact, all observed lines exhibit similar, view-dependent shifts; the analysis below only focuses on the IC line because of its relative spectral isolation and the limited impact of optical depth effects. Alongside plasma conditions inferred from line ratios, we take these line shift observations as conclusive evidence of solid-density plasma ablation.

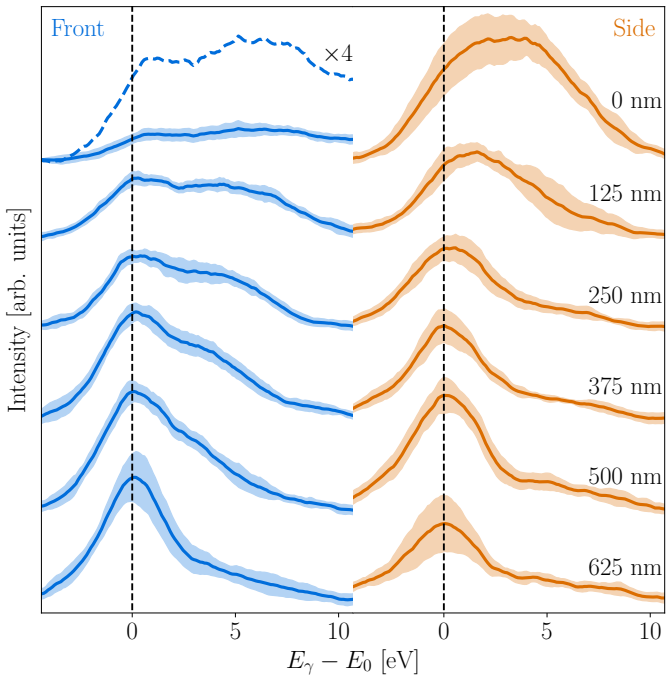

FIG. 2. IC line shapes from six noted depths z_{Ti} viewed from the front (left) and side (right). Solid lines and shaded regions are ten-shot intensity means and standard deviations. The untamped front-view line shape is expanded for clarity.

X-ray Doppler shifts are observed to vary with both depth z_{Ti} and viewing angle, as shown in Fig. 2. For untamped and shallow cases ($z_{\mathrm{Ti}} \leq 125$ nm), both front- and side-view spectra are blueshifted from the nominal IC line position $E_0 = 4726.9$ eV,[28] while front-view spectra maintain this blueshift for all $z_{\mathrm{Ti}} < 625$ nm. The front-view line shapes apparently comprise two overlapping peaks: the IC line and an evident shoulder several eV above E_0. The energy and intensity of the higher-energy component decrease with depth. Each line shape averages 10 independent shots and is background-subtracted by removing continuum emission and fitting Lorentzians to line emission on either distant side of the IC line; all quantitative claims herein are unperturbed when details of Lorentzian fitting are varied. Though IC line intensities are roughly constant for all buried layers from both views, untamped layers are outliers, as considered below.

Based on the observed Doppler shift trends, the velocities of ablating ions vary with depth. Velocity distributions $f(\boldsymbol{v})$ (where $|\boldsymbol{v}| \ll c$) are encoded in the line shapes and are extractable by forward modeling, as the observed line shape is a convolution of the hypothetical unshifted line emission with the distribution of ion velocities projected in the direction of observation. The most likely velocity distributions, vectorized with components v_n normal to the surface and $v_\parallel$ parallel to the surface, must be simultaneously consistent with line shapes observed from both front- and side-views.

Some fitting options, such as the degree to which a satellite is included in the unshifted line shape or the treatment of opacity effects, have small bearing on the below analysis. Varying the analysis details produced unanimously similar results with small quantitative changes only; conservative choices, such as assuming strong satellite contamination, have generated the results below. Fitting neglects plasma opacity, a small effect ($\tau < 0.5$ for the front-view IC line) that could broaden but cannot itself shift line shapes.

A Bayesian statistical approach fits the data using parameterized models for the vectorized velocity distribution. A Monte Carlo framework minimizes $\chi^2 = \sum_i (x_i - \tilde{x}_i)^2/\sigma_{xi}^2$, where x_i are experimentally measured intensities with ten-shot variance σ_{xi}^2, $\tilde{x}_i$ are intensities from the forward model, and i indexes spectral bins of front- and side-view line shapes; assuming that measurements are independent and normally distributed, the likelihood of obtaining the measurement with particular model parameters scales with $\exp\left(-\chi^2/2\right)$.[29] A nested sampling method, implemented in MultiNest[30] with a uniform prior distribution, determines the probability distributions of all model parameters with a well-defined stopping criterion.

By attempting this analysis with two separate models, one too simple and one sufficient to reproduce the data, we learn that ablating ions flow outward with two distinctly different velocities. First, the simpler "one-Gaussian" model assumes that velocity distributions f are flowing Maxwellians in each direction v_n and $v_\parallel$, each with a mean flow and thermal width. Second, the "two-Gaussian" model builds on the first by including an additional flowing Gaussian in $f(v_n)$ with its own mean, width, and relative amplitude. Figs. 3(a) and (b) show the most probable $f(v_n)$ and the corresponding synthetic front-view line shapes, respectively, for both models at $z_{\mathrm{Ti}} = 250$ nm. The flexibility of the two-Gaussian model is required for data fitting, evident both by eye and quantitatively ($\chi^2/(\#\text{ bins}) < 1$). The apparent shoulder in the measured line shape cannot be replicated unless the emission-weighted velocity distribution in the normal direction $f(v_n)$ has a second flowing component.

Since the analysis reveals a distinct, outward-ablating ion population at all locations $z_{\mathrm{Ti}} \leq 500$ nm, ablation velocity can be characterized as a function of depth. Mean velocities of slow and fast ion populations in all cases are shown in Fig. 3(c). The slower ion population has a uniformly low velocity except in the untamped case, whereas the faster population flows away from the surface at 200–500 km/s; the magnitude of the faster velocity decreases monotonically with depth. Notably, plasmas of He-like Ti (mass m_i, charge $Z = 20$) at the measured T_e have sound speeds[31] $c_s = \sqrt{\gamma Z k T_e/m_i} = 300 \pm 30$ km/s, a range that overlaps the velocity of the faster population in lightly tamped cases. (Though its value in dense plasmas is not well constrained,[32,33] we assume an adiabatic

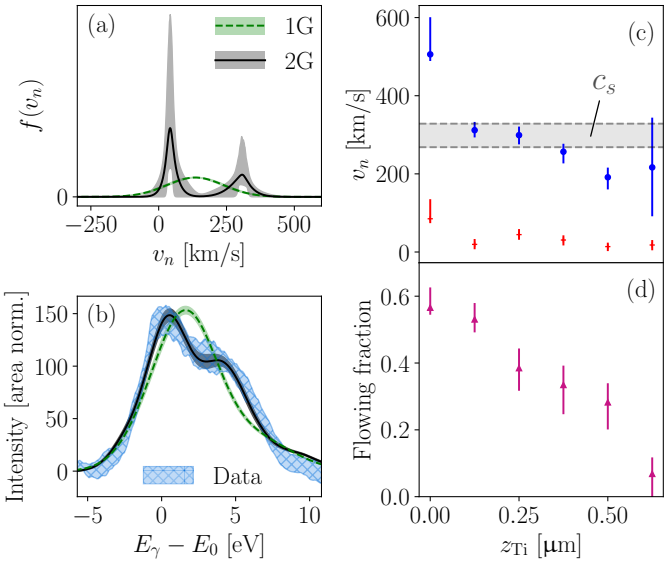

FIG. 3. (a) Normal-direction velocity distributions for $z_{\mathrm{Ti}} = 250$ nm fit from the one-Gaussian (1G) and two-Gaussian (2G) models. Shaded regions encompass 95% confidence intervals. (b) Best-fit line shapes corresponding to distributions in (a) overlaying the measurement. (c) Velocities of faster (•) and slower (+) peaks versus z_{Ti} with 98% confidence intervals, overlaid with inferred range of c_s. (d) Fraction of ions in the faster peak plotted as in (c).

index $\gamma = 1.5$; k is the Boltzmann constant.) We emphasize that the two ion populations, the nearly stationary one and the one flowing near c_s, are always well separated: few ions flow at intermediate velocities. Moreover, the presence of both slow (unablated) and fast (ablated) ions highlights that this measurement spans a transition from bulk solid to laser-ablated plume, encompassing the moment that ablation begins.

Ambiguity from time integration notwithstanding, the two distinct ion populations are most readily explained as occurring sequentially. Flowing ions cannot overlap the stationary population, as collisions would thermalize the distribution within ~ 10 fs,[31,34] less than the laser pulse duration. Neither is it likely that emission-weighting deemphasizes ions at intermediate velocities: no secondary energy source follows the laser pulse, so cooled ions cannot resume x-ray emission after accelerating. Instead, the solid-density plasma appears to rapidly accelerate from a near standstill to c_s, a speed which is essentially maintained for the remainder of the measurement.

Crucially, observed ion velocity distributions directly imply an electrostatic potential profile ϕ with a *step*, not a ramp, even though the latter has been generally understood to initiate plasma rarefaction. Ions ablating via a ramp-like ϕ would accelerate continuously, passing through many velocities; instead, this line shape analysis reveals that ions ablate at c_s, demanding a brief period of acceleration—a step in ϕ. This interpretation contradicts nearly all commonly accepted models of ablation,[12,35–38] analytical and computational, which characterize relativistic ion acceleration but do not replicate steps in ϕ that would be compatible with the data shown here. (A notable exception involving anomalous rarefaction shocks requires unrealistically high relativistic electron densities.[39,40]) This discrepancy implies that key models of high-intensity laser ablation miss essential physics relevant to the solid-density region.

As a final observation, we note that the fraction of ions flowing near c_s is $> 50\%$ at the surface and falls monotonically to zero by $z_{\mathrm{Ti}} = 625$ nm (Fig. 3(d)). The simplest hypothesis for this changing fraction is that near-surface ions spend more time flowing outward than deeper ones do; that is, ions accelerate to c_s earlier at the surface and later with increasing z_{Ti}. From this perspective, the velocity distributions inferred from Doppler-shifted line shapes are consistent with an ablation front, beginning at the laser-facing surface and traveling inward, that pulls unexpanded plasma outward with a step-like drop in ϕ toward the vacuum. This effect would not be driven by relativistic electrons or the MV-scale fields they produce, but rather by the dense, thermal plasma that determines c_s and therefore the magnitude of the kV-scale accelerating potential.

These features, ion flow at c_s and a sudden drop in ϕ, are reminiscent of plasma sheaths, or boundaries in ϕ that partition plasma regimes.[41] Sheaths build naturally at interfaces,[42] such as that between vacuum and laser-heated solid, with characteristic sizes in width and electrostatic potential that depend on bulk plasma conditions. It is typical for sheaths to accelerate ions to speeds near c_s (often called the "Bohm velocity" in this context). Measurements presented here support that a sheath-like structure exists at the laser-heated solid-vacuum interface; this structure seems to drive the initial disassembly of the solid-density plasma.

Though expansion is the end result of laser heating, many mechanisms driven by ultraintense photon pressure at the critical surface initially push plasma inward. According to some particle-in-cell modeling,[13,43] these plasma-pushing effects can drive compressional flows down to and through solid-density material. However, the outward flows seen here via Doppler blueshifts, not redshifts, explicitly contradict solid-density plasma compression via ion shocks[6,44] or hole-boring. Our findings therefore support theoretical limits on hole-boring density,[14] which would forbid laser-driven compression at densities above solid ($> n_S$) provided that laser reflectivity R is sufficiently low: $R \lesssim 0.2$.

The extreme temporal contrast of the ALEPH laser guarantees that the unexpected characteristics of ablation are not induced by the plasma prepulse. A recent third-order autocorrelator measurement of the fundamental ($\lambda = 800$ nm) laser pulse recorded the pre-

peak intensity rise over hundreds of ps. Assuming as usual that frequency doubling squares the laser contrast, this measurement excludes ionization of the target, which occurs around intensities of 6×10^{14} W/cm^2 at $\lambda = 400$ nm,[4] until 500 fs before maximum intensity at time t_0. A radiation-hydrodynamic simulation, assuming inverse Bremsstrahlung absorption with the measured laser intensity from time $t = t_0 - 500$ fs onward as input, was performed with the FLASH code.[45] The simulation predicted no disturbance deeper than 50 nm under the initial target surface. Direct laser interaction with the untamped $z_{\mathrm{Ti}} = 0$ nm layer is the probable cause of its unusually high ablation speed, 500 km/s $> c_s$, as well as the difference in intensity between front and side views there (preablated plasma may be elongated such that a larger volume is visible from the side). For all other cases, however, this simulation implies the observed ion ablation derives from the high-intensity pulse only, and that laser energy deposition was identical for $z_{\mathrm{Ti}} \geq 125$ nm.

In summary, analysis of Doppler-shifted x-ray line shapes has captured for the first time the velocity distributions of solid-density ions during ablation by an ultrarelativistic laser. This new capability, accomplished with high-resolution x-ray spectrometers, a laser system with extreme temporal contrast, and targets with thin tracer layers, establishes that ablating ions rapidly accelerate to the plasma sound speed, in contradiction to many models predicting a more gradual process. The facts that (1) ions ablate at c_s and (2) this mechanism persists more than 500 nm into the solid are both new benchmarks for models of laser-solid ablation. Lastly, the line shape measurement and Bayesian analysis techniques shown here are widely applicable to other dense plasma experiments, potentially useful for backlighter characterization,[46] constraining the disassembly rate of isochorically heated targets,[47] and tracking shocks and bulk ion flows in inertial confinement fusion.[48]

This work was supported by the DOE Office of Science, Fusion Energy Sciences under Contract No. DE-SC0021246: the LaserNetUS initiative at Colorado State University's Advanced Beam Laboratory, and was performed under the auspices of the U.S. Department of Energy by Princeton Plasma Physics Laboratory under contract DE-AC02-09CH11466 and by Lawrence Livermore National Laboratory under contract DE-AC52-07NA27344. JJR acknowledges support of DoD Vannevar Bush Faculty Fellowship ONR award N000142012842. Software used in this work was in part developed by the DOE NNSA-ASC OASCR Flash Center at the University of Chicago.

[1] W. Yu, V. Bychenkov, Y. Sentoku, M. Yu, Z. Sheng, and K. Mima, Phys. Rev. Lett. **85**, 570 (2000).
[2] A. Y. Faenov, A. Magunov, T. Pikuz, I. Y. Skobelev, S. Gasilov, S. Stagira, F. Calegari, M. Nisoli, S. De Silvestri, L. Poletto, *et al.*, Laser Part. Beams **25**, 267 (2007).
[3] A. Macchi, M. Borghesi, and M. Passoni, Rev. Mod. Phys. **85**, 751 (2013).
[4] P. Gibbon and E. Förster, Plasma Phys. Control. Fusion **38**, 769 (1996).
[5] Y. Ping, R. Shepherd, B. Lasinski, M. Tabak, H. Chen, H. Chung, K. Fournier, S. Hansen, A. Kemp, D. Liedahl, *et al.*, Phys. Rev. Lett. **100**, 085004 (2008).
[6] K. Akli, S. Hansen, A. Kemp, R. Freeman, F. Beg, D. Clark, S. Chen, D. Hey, S. Hatchett, K. Highbarger, *et al.*, Phys. Rev. Lett. **100**, 165002 (2008).
[7] C. Brown, D. Hoarty, S. James, D. Swatton, S. Hughes, J. Morton, T. Guymer, M. Hill, D. Chapman, J. Andrew, *et al.*, Phys. Rev. Lett. **106**, 185003 (2011).
[8] J.-L. Bobin, Phys. Rep. **122**, 173 (1985).
[9] J. Schou, S. Amoruso, and J. G. Lunney, *Laser Ablation and its Applications*, edited by C. Phipps (Springer US, Boston, MA, 2007) pp. 67–95.
[10] G. F. Indorf, G. G. Scott, M. A. Ennen, P. Forestier-Colleoni, D. Haddock, S. J. Hawkes, L. Scaife, N. Bourgeois, D. Symes, C. Thornton, *et al.*, Plasma Phys. Control. Fusion **64**, 034004 (2022).
[11] J. Crow, P. Auer, and J. Allen, J. Plasma Phys. **14**, 65 (1975).
[12] P. Mora, Phys. Rev. Lett. **90**, 185002 (2003).
[13] Y. Ping, A. Kemp, L. Divol, M. Key, P. Patel, K. Akli, F. Beg, S. Chawla, C. Chen, R. Freeman, *et al.*, Phys. Rev. Lett. **109**, 145006 (2012).
[14] N. Iwata, S. Kojima, Y. Sentoku, M. Hata, and K. Mima, Nature Comm. **9**, 1 (2018).
[15] Y. Wang, S. Wang, A. Rockwood, B. M. Luther, R. Hollinger, A. Curtis, C. Calvi, C. S. Menoni, and J. J. Rocca, Optics Lett. **42**, 3828 (2017).
[16] D. Rusby, L. Wilson, R. Gray, R. Dance, N. Butler, D. MacLellan, G. Scott, V. Bagnoud, B. Zielbauer, P. McKenna, *et al.*, J. Plasma Phys. **81** (2015).
[17] A. Moreau, R. Hollinger, C. Calvi, S. Wang, Y. Wang, M. G. Capeluto, A. Rockwood, A. Curtis, S. Kasdorf, V. Shlyaptsev, *et al.*, Plasma Phys. Control. Fusion **62**, 014013 (2019).
[18] P. Nilson, W. Theobald, J. Myatt, C. Stoeckl, M. Storm, J. Zuegel, R. Betti, D. Meyerhofer, and T. Sangster, Phys. Rev. E **79**, 016406 (2009).
[19] N. Woolsey, R. Clarke, D. Doria, L. Gizzi, G. Gregori, P. Hakel, S. Hansen, P. Koester, L. Labate, T. Levato, *et al.*, High Energy Density Phys. **7**, 105 (2011).
[20] L. Huang, M. Molodtsova, A. Ferrari, A. L. Garcia, T. Toncian, and T. Cowan, Phys. Plasmas **29**, 023102 (2022).
[21] B. Kraus, A. Chien, L. Gao, K. Hill, M. Bitter, P. Efthimion, H. Chen, M. Schneider, A. Moreau, R. Hollinger, *et al.*, Rev. Sci. Instrum. **92**, 033525 (2021).
[22] Y. E. Ralchenko, *Modern Methods in Collisional-Radiative Modeling of Plasmas*, Vol. 90 (Springer, 2016).
[23] V. Jacobs and M. Blaha, Phys. Rev. A **21**, 525 (1980).
[24] A. Gabriel, Mon. Notices Royal Astron. Soc. **160**, 99 (1972).
[25] S. Hansen, J. Bauche, C. Bauche-Arnoult, and M. Gu, High Energy Density Phys. **3**, 109 (2007).
[26] S. Stepanov, Proceedings SPIE: Advances in Computational Methods for X-ray and Neutron Optics **5536**, 16

(2004).
[27] S. Stepanov, "X-ray server," URL: https://x-server.gmca.aps.anl.gov.
[28] F. F. Goryaev, L. A. Vainshtein, and A. M. Urnov, At. Data Nuc. Data Tables **113**, 117 (2017).
[29] W. M. Bolstad and J. M. Curran, "Introduction to Bayesian Statistics," (John Wiley & Sons, 2016) Chap. 11.
[30] F. Feroz, M. Hobson, and M. Bridges, Mon. Notices Royal Astron. Soc. **398**, 1601 (2009).
[31] J. D. Huba, *NRL Plasma Formulary*, Vol. 6790 (Naval Research Laboratory, 1998).
[32] C. Fortmann, H. Lee, T. Döppner, R. Falcone, A. Kritcher, O. Landen, and S. Glenzer, Phys. Rev. Lett. **108**, 175006 (2012).
[33] E. Marenkov, D. Sinelnikov, N. Efimov, D. Bulgadaryan, and Y. M. Gasparyan, Phys. Plasmas **29**, 013509 (2022).
[34] B. Trubnikov, Rev. Plasma Phys. **1** (1965).
[35] P. Mora and T. Grismayer, Phys. Rev. Lett. **102**, 145001 (2009).
[36] T. Kiefer, T. Schlegel, and M. C. Kaluza, Phys. Rev. E **87**, 043110 (2013).
[37] D. Bara, M. Djebli, and D. Bennaceur-Doumaz, Laser and Particle Beams **32**, 391 (2014).
[38] I. Elkamash and I. Kourakis, Phys. Rev. E **94**, 053202 (2016).
[39] A. Diaw and P. Mora, Phys. Rev. E **84**, 036402 (2011).
[40] A. Diaw and P. Mora, Phys. Rev. E **86**, 026403 (2012).
[41] A. Sestero, Phys. Fluids **7**, 44 (1964).
[42] R. Franklin, J. Phys. D: Appl. Phys. **36**, R309 (2003).
[43] H. Habara, K. Lancaster, S. Karsch, C. Murphy, P. Norreys, R. Evans, M. Borghesi, L. Romagnani, M. Zepf, T. Norimatsu, *et al.*, Phys. Rev. E **70**, 046414 (2004).
[44] A. Turrell, M. Sherlock, and S. Rose, Nature Comm. **6**, 1 (2015).
[45] B. Fryxell, K. Olson, P. Ricker, F. Timmes, M. Zingale, D. Lamb, P. MacNeice, R. Rosner, J. Truran, and H. Tufo, Astrophys. J. Supp. Series **131**, 273 (2000).
[46] G. Hall, C. Krauland, M. Schollmeier, G. Kemp, J. Buscho, R. Hibbard, N. Thompson, E. Casco, M. Ayers, S. Ayers, *et al.*, Rev. Sci. Instrum. **90**, 013702 (2019).
[47] P. Nilson, J. Davies, W. Theobald, P. Jaanimagi, C. Mileham, R. Jungquist, C. Stoeckl, I. Begishev, A. Solodov, J. Myatt, *et al.*, Phys. Rev. Lett. **108**, 085002 (2012).
[48] R. Betti, K. Anderson, V. Goncharov, R. McCrory, D. Meyerhofer, S. Skupsky, and R. Town, Phys. Plasmas **9**, 2277 (2002).